



1       **Impact of using a new ultraviolet ozone absorption cross-section**  
2                               **dataset on OMI ozone profile retrievals**

3  
4               *Juseon Bak<sup>1</sup>, Xiong Liu<sup>1</sup>, Manfred Birk<sup>2</sup>, Georg Wagner<sup>2</sup>, Iouli E. Gordon<sup>1</sup>, and Kelly Chance<sup>1</sup>*

5                               <sup>1</sup>*Harvard-Smithsonian Center for Astrophysics, Cambridge, MA, USA*

6               <sup>2</sup>*Deutsches Zentrum für Luft- und Raumfahrt e.V. (DLR), Remote Sensing Technology Institute, Oberpfaffenhofen, D-*  
7                               *82234 Wessling, Germany*

8   **Abstract**

9       We evaluate different sets of high-resolution ozone absorption cross-section data for use in atmospheric  
10 ozone profile measurements in the Hartley and Huggins bands with a particular focus on Brion-Daumont-  
11 Malicet et al. (1995) (BDM) currently used in our retrievals, and a new laboratory dataset by Birk and  
12 Wagner (BW) (2018). The BDM cross-section data have been recommended to use for retrieval of ozone  
13 profiles using spaceborne nadir viewing Backscattered UltraViolet (BUV) measurements since its improved  
14 performance was demonstrated against other cross-sections including Bass and Paur (1985) (BP) and those  
15 of Serdyuchenko et al (2014) and Gorshelev et al. (2014) (SER) by the “Absorption Cross-Sections of  
16 Ozone” (ACSO) activity. The BW laboratory data were recently measured within the framework of the ESA  
17 project SEOM-IAS (Scientific Exploitation of Operational Missions - Improved Atmospheric Spectroscopy  
18 Databases) to provide an advanced absorption cross-section database. The BW cross-sections are made  
19 from measurements at more temperatures and in a wider temperature range than BDM, especially for low  
20 temperatures. Compared to BW, BDM cross-sections are positively biased from ~2 % at shorter UV to ~5 %  
21 at longer UV at warm temperatures. Furthermore, these biases dynamically increase by up to ± 40 % at cold  
22 temperatures due to no BDM measurements below 218 K. We evaluate the impact of using different cross-  
23 sections on ozone profile retrievals from Ozone Monitoring Instrument (OMI) measurements.  
24 Correspondingly, this impact leads to significant differences in individual ozone retrievals by up to 50 % in  
25 the tropopause where the coldest atmospheric temperature is observed. Bottom atmospheric layers illustrate  
26 the significant change of the retrieved ozone values with biases of 20 % in low latitudes, which is not the  
27 case in high latitudes because the ozone retrievals are mainly controlled by a priori ozone information in  
28 high latitudes due to less photon penetration down to the lower troposphere. Validation with ozonesonde  
29 observations demonstrates that BW and BDM retrievals show altitude-dependent bias oscillations of similar  
30 magnitude relative to ozonesonde measurements, much smaller than those of both BP and SER retrievals.



31 However, compared to BDM, BW retrievals show significant reduction in standard deviation by up to 15 %,  
32 especially at the coldest atmospheric temperature. Such improvement is achieved mainly by the better  
33 characterization of the temperature dependence of ozone absorption.

## 34 1. Introduction

35 Accurate knowledge of the absorption cross-sections of ozone and their temperature dependence is  
36 essential for highly accurate measurements of atmospheric ozone (Orphal et al., 2016) as well as other trace  
37 gases affected by the strong ozone absorption such as BrO, NO<sub>2</sub>, SO<sub>2</sub>, and CH<sub>2</sub>O (e.g., Seo et al., 2019;  
38 Theys et al., 2017). In the laboratory, measuring ozone cross-sections which can meet high requirements  
39 for accurate ozone profile measurements is still challenging in covering a wide spectral range (at least 270-  
40 340 nm) at high-resolution (at least 0.01 nm) at a wide range of atmospheric temperatures (180-300 K). The  
41 difficulties range from reactivity of ozone to calibration standards. For instance, as discussed in the recent  
42 review by Hodges et al. (2019) the accepted calibration of ozone cross-sections at mercury line (Hearn  
43 1961) was in need of revision. In addition simultaneous measurements of ozone in microwave, infrared and  
44 ultraviolet regions are subject to uncertainties in the respective regions (see discussion in Birk et al. (2019)  
45 and Tyuterev et al. (2019) for instance). The need to evaluate existing cross-sections used for all  
46 atmospheric measurements of ozone and to make its recommendations initiated the “Absorption Cross-  
47 Section of Ozone (ACSO) activity” that was established in 2008 and conducted in two phases (2009-2011,  
48 2013) (Orphal et al., 2016). The ACSO activity shows the need to continue laboratory ozone cross-section  
49 measurements of highest quality.

50 Prior to ACSO activities, the available ultraviolet (UV) ozone-cross sections were thoroughly  
51 reviewed by Orphal (2002, 2003) and as a result three datasets of ozone cross-sections were found to be in  
52 agreement of 1-2 % with each other, including BP 1985 (Bass and Paur, 1985), BDM 1995 (Daumont et al.  
53 1992; Brion et al., 1993; Malicet et al., 1995), and Global Ozone Monitoring Spectrometer (GOME) flight  
54 model (Burrows et al., 1999) (GMFM). The BP dataset is no longer recommended for any atmospheric  
55 ozone measurements (Orphal et al., 2016), but still used to keep the long-term consistency of ground-based  
56 Dobson/Brewer total ozone records and spaceborne TOMS/OMI total ozone records (McPeters et al. 2015).  
57 These cross-sections were also included in the 2004 edition of the HITRAN database (Rothman et al., 2005)  
58 and remained unchanged in subsequent editions including HITRAN2016 (Gordon et al., 2017). Using  
59 GMFM is restricted to GOME measurements because these cross-sections were measured at GOME  
60 resolution (~0.2 nm). On the other hand, the high-resolution cross-sections of BDM were first applied by  
61 Liu et al. (2005) for GOME ozone profile retrievals in the literature. In Liu et al. (2007), these three datasets  
62 were thoroughly assessed to find the most suitable cross-sections for GOME ozone profile retrievals (290-



63 307 nm and 325-340 nm). As a result, they recommended using the BDM for ozone profile retrievals due  
64 to much smaller fitting residuals and better agreement with ozonesonde measurements. Such improvement  
65 is likely due to better spectral resolution and wavelength calibration of BDM than BP and GMFM. After  
66 that, the recommendation of BDM for satellite ozone profile retrievals has been officially made by the  
67 ACSO activities during the first phase (2009-2011) and the second phase (2013), respectively. The first  
68 activity was focused on the intercomparison between BDM and BP, while the second activity was  
69 additionally organized in response to the new publication of a high-resolution laboratory dataset covering  
70 the temperature range of 193 to 293 K in 10 degree step by Serdyuchenko et al (2014) and Gorshelev et al.  
71 (2014) (abbreviated as SER). In the framework of the ACSO activity, Liu et al. (2013) evaluated the impact  
72 of changing from BDM to SER on Ozone Monitoring Instrument (OMI) ozone profile retrievals (270-330  
73 nm). The recommendation of the BDM was made again for use in ozone profile retrievals. Recently, a new  
74 laboratory dataset was measured at the German Aerospace Center (DLR) within the framework of the ESA  
75 project SEOM-IAS (Scientific Exploitation of Operational Missions - Improved Atmospheric Spectroscopy  
76 Databases) in order to improve the atmospheric BUV retrievals from the TROPOspheric Monitoring  
77 Instrument (TROPOMI) on board the Sentinel 5-Precursor satellite (Birk and Wagner, 2018) (abbreviated  
78 as BW). A publication with more details on experiment and analysis is in preparation. This motivates us to  
79 investigate if the current recommendation could be replaced with the BW dataset. This work will also help  
80 making decision on what cross-sections should replace BP measurements in the HITRAN database.

81 This paper is organized as follows: Section 2 compares the quadratic coefficients in the parameterization  
82 of temperature dependence and evaluates the parameterized cross-sections against interpolated ones.  
83 Section 3 analyzes the differences in individual OMI retrievals due to different cross-sections, which are  
84 evaluated against ozonesonde observations in Section 4. This paper is finally summarized and discussed in  
85 Section 5.

## 86 **2. Comparison of BDM and BW**

87 The BW dataset is publicly available at <https://zenodo.org/record/1485588> along with some  
88 experimental descriptions. A detailed publication is planned to describe the details of the experimental setup  
89 and procedure so only a brief overview is given here. These cross-sections are given at six temperatures  
90 (193, 203, 233, 253, 273, and 293 K) and at vacuum wavelengths in the spectral range 244 to 346 nm,  
91 measured by means of Fourier-Transform Spectroscopy (FTS) at DLR at a spectral resolution of  $3.3 \text{ cm}^{-1}$   
92 (0.02-0.04 nm). A total of 191 measurements were recorded in two spectral ranges. Absorption cross-  
93 sections were obtained at each temperature by means of a global least squares fit. Below 285.71 nm,  
94 absorption cross-sections were smoothed to  $7.7 \text{ cm}^{-1}$  (0.04-0.06 nm) resolution by convolving with a



95 Gaussian to reduce the noise. Offset corrections were made for each of the 6 temperatures by fitting to  
96 SER dataset since it was measured at higher ozone column density and thus considered more reliable  
97 regarding offset. After offset correction polynomials of 1<sup>st</sup> order (<270.27 nm) and 2<sup>nd</sup> order (>270.27 nm)  
98 in temperature were fitted for each spectral point to improve the statistical uncertainty. The offset  
99 corrections have minor effect on the cross-sections except for wavelengths above ~330 nm. Figure 1.a  
100 illustrates BW measurements without polynomial fit in temperatures to be fairly compared with BDM  
101 measurements (Fig. 1.b) with respect to the dependence of cross-sections on wavelength and temperature.  
102 The BDM measurements are given at five temperatures (218, 228, 243, 273, and 295 K) and at air  
103 wavelengths over the spectral range 195-519 nm with spectral resolution of 0.01-0.02 nm. Note that the  
104 wavelengths of these measurements are converted to vacuum wavelengths in Figure 1.b.. Measured cross-  
105 sections are typically parameterized quadratically to be applied conveniently at any atmospheric  
106 temperatures using the following equation:

$$107 \quad C = C_0 + C_1(T - 273.15) + C_2(T - 273.15)^2 \quad (1)$$

108 The non-linear least squares fitting used in this paper converges typically within 3 iterations for both  
109 BDM and BW. Measurements at 273 K are excluded for the BDM quadratic temperature fitting, according  
110 to Liu et al. (2007). In Figure 2, the derived temperature dependent coefficients are illustrated, with their  
111 relative differences.  $C_0$  values are similar to each other in the Hartley band with relative biases of 2-3%.  
112 However, the Huggins band shows large spiky biases of up to 8%.  $C_1$  and  $C_2$  represent linear and  
113 quadratic temperature dependences of absorption cross-sections, respectively. The cross-sections in the  
114 Hartley band are almost independent of the temperature variation and thereby large differences of these  
115 coefficients between two datasets are due the large correlation between  $C_1$  and  $C_2$  and are of minor  
116 importance to the parameterized cross-sections. However, the Huggins band shows the distinctly different  
117 temperature dependence between two cross-section datasets, especially for the quadratic terms. For  $C_2$ , the  
118 BW data show more monotonic wavelength dependence in the range 290-310 nm. Note that we determined  
119 that the parameterization schemes used in this work and Birk and Wagner (2018) are very similar by the  
120 fact that no residuals remain when comparing BW cross-sections with these two schemes (not shown here).  
121 Figure 3 compares the residuals of the fitted cross-sections relative to the original measurements  
122 interpolated to many atmospheric temperatures using a spline scheme. The BDM quadratic approximation  
123 has large positive residuals of up to 15 % for the temperatures ranging from 243 and 295 K due to  
124 insufficient sampling to account for the non-linearity of the temperature dependence, especially for the  
125 longer UV wavelength range. Moreover, approximating the BDM cross-sections at temperatures below 218  
126 K results in errors of  $\pm 5\%$  below 315 nm and up to  $\pm 40\%$  above. Compared to the BDM dataset, the



127 parameterization of BW cross-sections results into significantly reduced residuals, of 0.25% below 320 nm  
128 and typically less than 2% at longer wavelengths if the temperature is within the boundaries of the  
129 measurements. Residuals are within 5% even if the temperatures are out of the boundaries. This  
130 demonstrates that the temperatures of BW measurements are well selected to characterize the temperature  
131 dependence of ozone cross-sections, whereas cross-section errors due to the BDM parameterization exist.  
132 Figure 4 shows the direct comparison of parameterized cross-sections between BDM and BW. The  
133 difference of cross-sections between BDM and BW are generally consistent with the corresponding  
134 comparison of  $C_0$  around 270 K. The differences at different temperatures are typically within 2% for  
135 wavelengths below 310 nm except for several spikes around 276, 297, and 306 nm that are correlated with  
136 the differences of  $C_2$ . At wavelengths larger than 315 nm, the biases show large temperature dependence,  
137 with the bias range increasing from ~5% at 315 nm to ~20% at 340 nm.

### 138 3. Impact of using different cross sections on ozone profile retrievals

139 OMI ozone profiles are retrieved at 24 layers from BUUV spectra for 270-309 nm in UV1 and 312-330  
140 nm in UV2 using an optimal estimation technique (Liu et al. 2010). The implemented configurations in this  
141 work are similar to those in Liu et al. (2013). One orbit of measurements on 1<sup>th</sup> July 2006 is used to see  
142 how our retrievals are changed due to using different cross-sections. Figure 5 shows the response of our  
143 retrievals to the parameterization errors shown in Figure 3 as functions of solar zenith angle (SZA).  
144 Compared to the BDM, the ozone retrievals are almost independent of the BW parameterization errors,  
145 with individual differences of 2-3% below 20 km and ~0% above. The differences of the BDM cross-  
146 sections with and without the parameterization are -5 to 15% in the lower troposphere at smaller SZAs and  
147 up to  $\pm 20\%$  around 10 km at higher SZAs. The UV photon penetration down to the lower atmosphere  
148 decreases with SZAs increasing and thereby tropospheric ozone retrievals become insensitive due to cross-  
149 section errors at high SZAs, while a priori ozone information becomes more important to the retrieval.  
150 Figures 6-8 show the retrieval differences when parameterized BW and BDM cross-sections are  
151 implemented, respectively. To evaluate the different implementations, both fitting and retrieval accuracies  
152 are assessed. However, it is very hard to see large differences in fitting residuals at final iteration compared  
153 to differences on the retrieved elements of the state vector because the algorithm iteratively updates the  
154 state vector toward minimizing the differences in the spectral residuals. The fitting residuals are comparable  
155 at final iteration when applying BW and BDM dataset as shown in Figure 6.a except for noticeable smaller  
156 residuals in 310-320 nm. However, we can find the distinct change in the mean residuals of measured  
157 radiance to simulated radiance at initial iteration, mainly over the wavelength range of 290 to 315 nm, up  
158 to 5% as shown in Figure 6.b. On the other hand, Liu et al. (2007, 2013) demonstrated the distinct change



159 of final fitting residuals when changing BDM to BP and GMFM, implying that using BW dataset improves  
160 fitting accuracies over using BP and GMFM, but produces similar fitting accuracies to using BDM and  
161 SER. Figure 7 shows relative differences of the retrieved ozone profiles with the corresponding temperature  
162 profiles taken from the National Centers for Environmental Protection (NCEP) final (FNL) operational  
163 global analysis data. Large differences of 20-50% commonly exist along the tropopause, where the original  
164 BDM measurements could not cover atmospheric temperatures below 218 K. Some larger differences occur  
165 throughout the troposphere in the tropics likely due to the relative smaller retrieved partial ozone columns.  
166 The individual differences of retrieved ozone in the lower troposphere are  $\sim 20\%$ . Corresponding  
167 differences of total column ozone, from integrating retrieved ozone profiles, are also presented by the black  
168 line in Fig. 7a. Applying BDM causes an underestimation of total ozone except at the South Pole, despite  
169 the overestimation being prominent for the individual layer columns in the troposphere. The magnitude of  
170 this underestimation/overestimation is  $\sim 1\%$ , which is comparable to the overall accuracy ( $\sim 1.5\%$ ) of the  
171 OMI operational total ozone product against ground-based measurements (McPeters et al. 2015). The  
172 wavelength shifts between ozone cross-sections and radiances are iteratively and simultaneously fitted with  
173 ozone for their respective UV1 and UV2 channels. Figure 8 compares how the wavelengths of different  
174 cross-sections are adjusted in each fitting window at nadir view. According to Schenkeveld et al. (2017),  
175 wavelength errors of OMI radiances are expected to be  $\sim 0.002$  nm in UV2 and  $\sim 0.015$  in UV1. The fitted  
176 wavelength shifts fall in the ranges of the OMI wavelength accuracy. Compared to the BDM, the BW  
177 dataset has the relative shifts of  $\sim 0.002$  nm in the UV2. The mean shifts in the UV1 are comparable, 0.0087  
178 nm and 0.0081 nm for BDM and BW, respectively, whereas the variance of the fitted shifts over the latitude  
179 is reduced with the use of BW dataset as the shifts are more stable south of  $30^\circ\text{S}$ . On the other hand, Liu et  
180 al. (2013) shows that the relative shifts between SER and BDM are  $\sim 0.007$  nm in both UV1 and UV2, and  
181 BP shifts vary largely with latitude by up 0.01 nm. These results indirectly demonstrate the similarity of the  
182 wavelength calibration quality between BDM and BW measurements.

183

#### 184 **4. Validation with ozonesonde observations**

185 Ozonesonde measurements at five stations during the period 2005 to 2008 are used to evaluate the  
186 retrieval accuracy of ozone profile retrievals using different cross-sections. In addition to the currently used  
187 BDM and the new BW datasets, BP and SER previously assessed in Liu et al. (2013) are included in this  
188 evaluation. Typically, high-resolution vertical structures of ozonesonde profiles ( $\sim 100$  m) are degraded to  
189 OMI resolution (6-10 km in the stratosphere, 10-15 km in the troposphere) using retrieval averaging kernels  
190 to eliminate the effect of OMI smoothing errors (80% of total retrieval errors in the lower stratosphere and  
191 troposphere) in comparison with ozonesondes; as a result, the standard deviations of comparisons are



192 typically reduced by a factor of 2 in the troposphere and lower stratosphere while the comparisons of mean  
193 biases are less impacted by using OMI smoothing errors or not. In this paper, the conclusion on which cross-  
194 section data should be used stays the same no matter whether ozonesonde profiles are vertically smoothed  
195 or not, so we present validation results only using original ozonesonde measurements. In Figure 9, mean  
196 biases of the retrieved ozone profiles relative to ozonesondes and the corresponding standard deviations are  
197 presented at each station, arranged by latitude from north to south, together with corresponding temperature  
198 profiles.

199 In layers above ~20 km, a negligible impact of using different cross-sections is found because the  
200 measurement information comes mainly from the Hartley ozone absorption band with little dependence on  
201 temperature variation. Both BP and SER measurements provide a wider temperature range and more  
202 samplings than BDM, but switching from BDM to BP / SER results in large altitude-dependent oscillations  
203 of mean biases below ~20 km and noticeably fewer successful retrievals, consistent with Liu et al. (2013).  
204 These oscillations tend to be wider with the minimum atmospheric temperatures decreasing such that the  
205 mean biases increase  $\pm 50\%$  at mid/high latitudes (210-215 K) to  $\pm 70\%$  at low latitudes (200-205 K), which  
206 is partly due to smaller ozone concentration in the tropics and hence the larger relative differences. This  
207 result implies a defect in accounting for the temperature dependence in both the BP/SER cross-section  
208 datasets, especially in the lower temperature range. Using BDM and BW cross-sections generally show  
209 much smaller altitude-dependent oscillations of mean biases. The magnitudes of the biases are smaller for  
210 BDM for the two middle/high latitude stations, but smaller for BW at the other, lower latitude stations. The  
211 BW retrievals typically show negative biases of up to 30% relative to BDM retrievals. The number of  
212 successful BW retrievals is slightly smaller than that of BDM retrievals because the negative biases cause  
213 more occurrences of negative ozone so that the retrieval convergence is more difficult. It is difficult to  
214 determine which one is better for ozone profile retrievals from the mean biases as OMI radiances contain  
215 systematic radiometric calibration errors (Liu et al., 2010) and ozonesonde observations can also contain  
216 systematic measurement errors (Liu et al., 2006).

217 As seen from the comparison of standard deviations in the middle panels, the use of BW consistently  
218 gives significantly smaller standard deviations, by 5-20% in the lower stratosphere and upper troposphere  
219 except for the high latitude station, Sodankyla. BW, BDM, and SER retrievals show similar standard  
220 deviations at this station probably due to relatively warmer temperature, ~210-220 K in this altitude range.  
221 In Figure 10, individual differences of layer column ozone between OMI retrievals and ozonesondes using  
222 BDM and BW datasets are plotted as a function of temperatures for 8 layers below ~20 km. In this  
223 comparison, the noticeable reduction of the scatter between OMI and ozonesonde, by 5-15% at layers from



224 17 to 8.5 km as well as by a few % below or above them, after applying BW cross-sections is further evident.  
225 Improvements of the retrieval precision corresponding to standard deviations have been less often achieved  
226 than those of the retrieval accuracy corresponding to mean biases; for examples, systematic errors in ozone  
227 profile retrievals could be reduced by accounting for polar mesospheric clouds (Bak et al. 2016) and slit  
228 function errors (Bak et al. 2019) as well as applying empirical calibration (Bak et al. 2017) whereas the  
229 reduction of the standard deviations was achieved only in Bak et al. (2013) by better representing  
230 dynamically induced ozone variability in the a priori ozone. This significant improvement in standard  
231 deviations indicates that temperature dependence is better characterized at the lower temperatures near  
232 ~200K by the BW dataset.

233

## 234 5. Summary and discussion

235 This paper evaluates the recently measured laboratory high-resolution BW (2018) ozone cross-section data  
236 within the framework of the ESA project SEOM-IAS to see whether or not the current recommendation  
237 could be changed for improving ozone profile retrievals from UV measurements. The BDM (1993) dataset  
238 has been regarded as the standard ozone absorption cross-section in space-based ozone profile retrievals  
239 from BUUV measurements: thereby we focused on comparing BW and BDM datasets and their impact on  
240 our ozone profile retrievals from OMI BUUV measurements. Compared to BDM given at 5 temperatures  
241 ranging from 218 to 295 K, the BW dataset provides improved temperature coverage of 193 to 293 K, every  
242 20 K. To conveniently apply the cross-section measurements at any temperature, we quadratically  
243 parameterized its temperature dependence using iterative non-linear least squares fitting. The 273 K  
244 measurements are excluded in the BDM parameterization to improve the fitting residuals at other  
245 temperatures. However, the BDM parameterization causes increasing biases in approximate cross-sections  
246 at lower temperatures using their 243 and 218 K measurements, especially at longer wavelengths in the  
247 Huggins band (up to 20%). It reveals serious errors of up to  $\pm 40\%$  in representing the values at lower  
248 temperatures out of the BDM measurements. In comparison, the BW approximation is very closely  
249 parameterized to the original data, typically within 2%, while most of the atmospheric temperatures are  
250 covered by the BW dataset; the biases increase to  $\pm 5\%$  at temperatures below 195 K. Correspondingly,  
251 individual ozone profile retrievals show less sensitivity due to the BW parameterization errors, with biases  
252 of  $\sim 2\%$  or less over the altitude range. On the other hand, using the parameterized BDM causes biases of  
253 5-10% at bottom layers in the low latitudes and 10-20% at the tropopause. Relative to the BDM dataset, the  
254 BW data show systematic biases of 2-3% in  $C_o$  at shorter wavelengths below 300 nm, but larger spiky



255 biases of up to 8% at wavelengths longer than 315 nm. The difference in  $C_1$  and  $C_2$  implies distinctly  
256 different temperature dependence especially in non-linearity in the Huggins bands. We then compared  
257 ozone profile retrievals from one orbit of OMI measurements with BW and BDM cross-section datasets.  
258 Using different datasets gives comparable results in the wavelength shift of cross-sections relative to OMI  
259 radiance wavelengths and fitting residuals at the final iteration, respectively. However, the initial iteration  
260 gives ~5% differences in fitting residuals near 290-315 nm, which results in significant differences of the  
261 adjusted ozone profiles at the final iteration, ~50% at the tropopause across most latitudes and ~20% at the  
262 bottom layers in the low-latitudes. To evaluate the quality of ozone retrievals, ozonesonde measurements  
263 are compared at five stations. In this validation, we include other cross-section datasets, BP (1985) and SER  
264 (2014). Compared to the large vertical oscillation of mean biases for OMI ozone profiles using BP and SER,  
265 the BW retrievals show mean biases comparable to or sometimes improved over the BDM retrievals. The  
266 most important improvement due to switching from BDM to BW is the significant reduction of the standard  
267 deviations, by up to 15% in the lower stratosphere and upper troposphere where atmospheric temperatures  
268 are lower than ~200K.

269 Based on this evaluation, switching our ozone absorption cross-section reference from BDM to BW is  
270 very promising for OMI ozone profile retrievals. However, in this evaluation soft calibration is turned off  
271 and thereby the final decision on our algorithm will be made after further evaluating our retrievals with  
272 BW-based soft calibration. In order to make a robust recommendation it might be useful for the ACSO  
273 committee to organize another activity to assess the impact of applying this new dataset on other ozone  
274 measurements on column ozone or profiles from various platforms. The results of this work in addition to  
275 that of Orphal et al. (2016) will help the HITRAN committee to decide which cross-sections should be  
276 included in HITRAN2020 edition.

277 Using different ozone cross-sections could also cause an important change in SO<sub>2</sub> retrievals fitted in the  
278 Huggins band and therefore it the impact of applying both ozone and SO<sub>2</sub> cross-sections available from the  
279 BW datasets (<https://zenodo.org/record/1492582>) should be evaluated. However, the spectral coverage of  
280 the BW dataset is insufficient for the spectral fitting of other trace gases such as BrO and HCHO, both of  
281 which have significant interference with ozone. Ozone cross-sections in other wavelength ranges, such as  
282 the mid-infrared region near 9.6 μm and the Chappuis band (400-650 nm), have not been thoroughly  
283 evaluated in the literature. The ozone profile algorithm used in this work will be implemented for the  
284 Tropospheric Emissions: Monitoring of Pollution (TEMPO) satellite combining the UV and visible  
285 measurements to improve the detection of boundary layer ozone. Therefore we should extend this work to  
286 find the most suitable ozone cross-sections in the TEMPO visible ozone channel (540-740 nm), focusing



287 on SER 2014 covering from 213 to 1100 nm (193-293 K in 10K steps) and that of Brion et al. (1998) which  
288 provides measurements at 218 and 295 K from ~520 nm to ~650 nm. Moreover, the need to improve wide  
289 spectral range laboratory cross-section measurements of ozone is still required to advance atmospheric  
290 ozone and other trace gases measurements.

291 **Author contributions.** JB and XL designed the research; MB and GW provided oversight and guidance for analyzing  
292 cross-section dataset; XL contributed to analyzing ozone profile retrievals; JB conducted the research and wrote the  
293 paper; IG and KC contributed to the analysis and writing.

294

295 **Competing interests.** The authors declare that they have no conflicts of interest.

296

297 **Data availability,** The BW cross-section dataset is available at <https://zenodo.org/record/1485588>. OMI  
298 Level1b radiance datasets are available at [https://aura.gesdisc.eosdis.nasa.gov/data/Aura\\_OMI\\_Level1/](https://aura.gesdisc.eosdis.nasa.gov/data/Aura_OMI_Level1/)  
299 (last access: 31 Nov 2019). The ozonesonde data used to validate our ozone profile retrievals were obtained  
300 through the WOUDC and SHADOZ. The WOUDC dataset is available at  
301 <https://woudc.org/data/products/ozonesonde/> (last access: 31 Nov 2019) and for the SHADOZ dataset at  
302 <https://tropo.gsfc.nasa.gov/shadoz/Archive.html> (last access: 31 Nov 2019).

303

304 **Acknowledgement,** We acknowledge the OMI science team for providing their satellite data and the  
305 WOUDC and SHADOZ networks for their ozonesonde datasets. Research at the Smithsonian Astrophysical  
306 Observatory by Juseon Bak, Xiong Liu, and Kelly Chance was funded by the NASA Aura science team  
307 program (NNX17AI82G). MB and GW thank the European Space Agency (ESA) for funding of the SEOM-  
308 IAS project (ESA/AO/1-7566/13/I-BG).

309

310 **Financial support.** This research has been supported by NASA Aura science team program (grant no.  
311 NNX17AI82G). The SEOM-IAS project has been funded by ESA (ESA/AO/1-7566/13/I-BG).

312

313

## References

- 314 Bak, J., Liu, X., Kim, J. H., Deland, M. T., and Chance, K.: Improvement of OMI ozone profile retrievals  
315 by simultaneously fitting polar mesospheric clouds, *Atmos. Meas. Tech.*, 9, 4521–4531,  
316 <https://doi.org/10.5194/amt-9-4521-2016>, 2016.
- 317 Bak, J., Liu, X., Kim, J.-H., Haffner, D. P., Chance, K., Yang, K., and Sun, K.: Characterization and  
318 correction of OMPS nadir mapper measurements for ozone profile retrievals, *Atmos. Meas. Tech.*, 10,  
319 4373–4388, <https://doi.org/10.5194/amt-10-4373-2017>, 2017



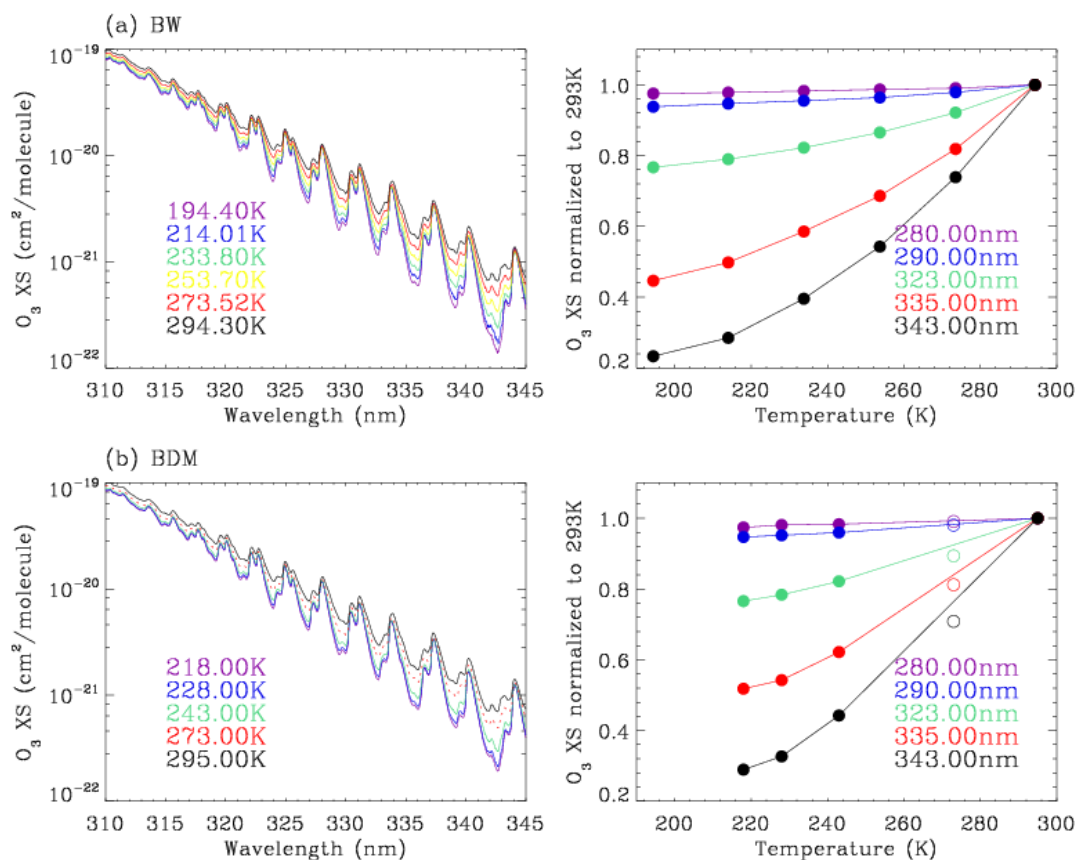
- 320 Bak, J., Liu, X., Sun, K., Chance, K., and Kim, J.-H.: Linearization of the effect of slit function changes for  
321 improving Ozone Monitoring Instrument ozone profile retrievals, *Atmos. Meas. Tech.*, 12, 3777–3788,  
322 <https://doi.org/10.5194/amt-12-3777-2019>, 2019.
- 323 Bak, J., Liu, X., Wei, J. C., Pan, L. L., Chance, K., and Kim, J. H.: Improvement of OMI ozone profile  
324 retrievals in the upper troposphere and lower stratosphere by the use of a tropopause-based ozone profile  
325 climatology, *Atmos. Meas. Tech.*, 6, 2239–2254, doi:10.5194/amt-6-2239-2013, 2013.
- 326 Bass, A. M. and Paur, R. J.: The ultraviolet cross-sections of ozone. I. The measurements, II –  
327 Results and temperature dependence, in: *Atmospheric ozone; Proceedings of the Quadrennial*,  
328 1, 606–616, 1985.
- 329 Birk, M. and Wagner, G.: ESA SEOM-IAS – Measurement and ACS database O3 UV region (V  
330 ersion I) [Data set]. Zenodo. <http://doi.org/10.5281/zenodo.1485588>, 2018.
- 331 Birk, M., Wagner, G., Gordon, I. E., & Drouin, B. J.: Ozone intensities in the rotational bands. *Journal of*  
332 *Quantitative Spectroscopy and Radiative Transfer*, 226, 60–65.  
333 <https://doi.org/10.1016/J.JQSRT.2019.01.004>, 2019
- 334 Brion, J., Chakir, A., Daumont, D., Malicet, J., and Parisse, C.: High-resolution laboratory absorp  
335 tion cross section of O<sub>3</sub>. Temperature effect, *Chem. Phys. Lett.*, 213, 610–612, 1993.
- 336 Brion, J., Chakir, A., Charbonnier, J., Daumont, D., Parisse, C., Malicet, J.: Absorption spectra  
337 measurements for the ozone molecule in the 350–830 nm region, *J. Atmos. Chem.* 30 (1998) 291–99,  
338 1998.
- 339 Burrows, J. P., Dehn, A., Deters, B., Himmelmann, S., Richter, A., Voigt, S., and Orphal, J.: Atmospheric  
340 remote-sensing reference data from GOME: Part 2. Temperature-dependent absorption cross-sections  
341 of O<sub>3</sub> in the 231–794 nm range, *J. Quant. Spectrosc. Radiat. Transfer*, 61(4), 509–517, 1999.
- 342 Daumont, Brion, J., Charbonnier, J., and Malicet, J.: Ozone UV spectroscopy I: Absorption crosssections  
343 at room temperature, *J. Atmos. Chem.*, 15, 145–155, 1992.
- 344 Gordon, I., Rothman, L., Hill, C., Kochanov, R., Tan, Y., Bernath, P., Birk, M., Boudon, V., Campargue, A.,  
345 Chance, K., Drouin, B., Flaud, J.-M., Gamache, R., Hodges, J., Jacquemart, D., Perevalov, V., Perrin,  
346 A., Shine, K., Smith, M.-A., Tennyson, J., Toon, G., Tran, H., Tyuterev, V., Barbe, A., Császár, A.,  
347 Devi, V., Furtenbacher, T., Harrison, J., Hartmann, J.-M., Jolly, A., Johnson, T., Karman, T., Kleiner,  
348 I., Kyuberis, A., Loos, J., Lyulin, O., Massie, S., Mikhailenko, S., Moazzen-Ahmadi, N., Müller, H.,  
349 Naumenko, O., Nikitin, A., Polyansky, O., Rey, M., Rotger, M., Sharpe, S., Sung, K., Starikova, E.,  
350 Tashkun, S., Auwera, J. V., Wagner, G., Wilzewski, J., Wcisło, P., Yu, S., and Zak, E.: The  
351 HITRAN2016 molecular spectroscopic database, *J. Quant. Spectrosc. Ra.*, 203, 3–69,  
352 <https://doi.org/10.1016/j.jqsrt.2017.06.038>, 2017.
- 353 Hearn, A. G.: The absorption of ozone in the ultra-violet and visible regions of the spectrum. *Proceedings*  
354 *of the Physical Society*, 78(5), 932–940. <https://doi.org/10.1088/0370-1328/78/5/340>, 1961.
- 355 Hodges, J. T., Viallon, J., Brewer, P. J., Drouin, B. J., Gorshelev, V., Janssen, C., et al.: Recommendation of  
356 a consensus value of the ozone absorption cross-section at 253.65 nm based on a literature review.



- 357 Metrologia, 56(3), <https://doi.org/10.1088/1681-7575/ab0bdd>, 2019
- 358 Gorshchev, V., A. Serdyuchenko, M. Weber, W. Chehade, and J. P. Burrows, High spectral resolution ozone  
359 absorption cross-sections – Part 1: Measurements, data analysis and comparison with previous  
360 measurements around 293 K, Atmos. Meas. Tech., 7, 609–624, doi:10.5194/amt-7-609-2014, 2014.
- 361 McPeters, R. D., Frith, S., and Labow, G. J.: OMI total column ozone: extending the long-term data record,  
362 Atmos. Meas. Tech., 8, 4845–4850, <https://doi.org/10.5194/amt-8-4845-2015>, 2015.
- 363 Liu, C., Liu, X., and Chance, K.: The impact of using different ozone cross sections on ozone profile  
364 retrievals from OMI UV measurements, J. Quant. Spectrosc. Ra., 130, 365–372,  
365 doi:10.1016/j.jqsrt.2013.06.006, 2013.
- 366 Liu, X., Chance, K., Sioris, C. E., and Kurosu, T. P.: Impact of using different ozone cross sections on  
367 ozone profile retrievals from Global Ozone Monitoring Experiment (GOME) ultraviolet  
368 measurements, Atmos. Chem. Phys., 7, 3571–3578, doi:10.5194/acp-7-3571-2007, 2007.
- 369 Liu, X., Chance, K., Sioris, C. E., and Kurosu, T. P., Newchurch, M. J.: Intercomparison of GOME,  
370 ozonesonde, and SAGE II measurements of ozone: Demonstration of the need to homogenize available  
371 ozonesonde data sets, J. Geophys. Res. 111 (D14) D14305, doi:10.1029/2005JD006718, 2006..
- 372 Liu, X., Chance, K., Sioris, C. E., Spurr, R. J. D., Kurosu, T. P., Martin, R. V., and Newchurch, M. J.:  
373 Ozone profile and tropospheric ozone retrievals from Global Ozone Monitoring Experiment:  
374 algorithm description and validation, J. Geophys. Res., 110, D20307, doi: 10.1029/2005JD006240,  
375 2005.
- 376 Liu, X., Bhartia, P. K., Chance, K., Spurr, R. J. D., and Kurosu, T. P.: Ozone profile retrievals from the ozone  
377 monitoring instrument. Atmos. Chem. Phys., 10, 2521–2537, 2010.
- 378 Malicet, Daumont, D., Charbonnier, J., Parisse, C., Chakir, A., and Brion, J.: Ozone UV spectros  
379 copy. II. Absorption cross-sections and temperature dependence, J. Atmos. Chem, 21, 263–27  
380 3, 1995.
- 381 Rothman, L. S., Jacquemart, D., Barbe, A., Chris Benner, D., Birk, M., Brown, L. R., et al.: The HITRAN  
382 2004 molecular spectroscopic database. *Journal of Quantitative Spectroscopy and Radiative Transf*  
383 *er*, 96(2), 139–204. <https://doi.org/10.1016/j.jqsrt.2004.10.008>, 2005.
- 384 Schenkeveld, V. M. E., Jaross, G., Marchenko, S., Haffner, D., Kleipool, Q. L., Rozemeijer, N.  
385 C., Veeffkind, J. P., and Levelt, P. F.: In-flight performance of the Ozone Monitoring Instru  
386 ment, Atmos. Meas. Tech., 10, 1957–1986, <https://doi.org/10.5194/amt-10-1957-2017>, 2017.
- 387 Seo, S., Richter, A., Blechschmidt, A.-M., Bougoudis, I., and Burrows, J. P.: First high-resolution BrO  
388 column retrievals from TROPOMI, Atmos. Meas. Tech., 12, 2913–2932, [https://doi.org/10.5194/amt-](https://doi.org/10.5194/amt-12-2913-2019)  
389 [12-2913-2019](https://doi.org/10.5194/amt-12-2913-2019), 2019.
- 390 Serdyuchenko, A., Gorshchev, V., Weber, M., Chehade, W., and Burrows, J. P.: High spectral resolution  
391 ozone absorption cross-sections – Part 2: Temperature dependence, Atmos. Meas. Tech., 7, 625–636,  
392 <https://doi.org/10.5194/amt-7-625-2014>, 2014.
- 393 Orphal, J.: A critical review of the absorption cross-sections of O<sub>3</sub> and NO<sub>2</sub> in the 240–790 nm region, Part  
394 1. ozone, in ESA Technical Note MO-TN-ESA-GO-0302, ESA-ESTEC, Noordwijk, The Netherlands,



- 395           2002.
- 396   Orphal, J.: A critical review of the absorption cross-sections of O<sub>3</sub> and NO<sub>2</sub> in the 240–790 nm region, J.  
397       Phtotochem. Photobiol. A., 157, 185–209, 2003.
- 398   Orphal, J., Staehelin, J., Tamminen, J., et al.: Absorption crosssections of ozone in the ultraviolet and visible  
399       spectral regions: Status report 2015, J. Mol. Spectrosc., 327, 105–121,  
400       <https://doi.org/10.1016/j.jms.2016.07.007>, 2016.
- 401   Theys, N., De Smedt, I., Yu, H., Danckaert, T., van Gent, J., Hörmann, C., Wagner, T., Hedelt, P., Bauer, H.,  
402       Romahn, F., Pedernana, M., Loyola, D., and Van Roozendael, M.: Sulfur dioxide retrievals from  
403       TROPOMI onboard Sentinel-5 Precursor: algorithm theoretical basis, Atmos. Meas. Tech., 10, 119–  
404       153, <https://doi.org/10.5194/amt-10-119-2017>, 2017.
- 405   Tyuterev, V. G., Barbe, A., Jacquemart, D., Janssen, C., Mikhailenko, S. N., & Starikova, E. N.: Ab initio  
406       predictions and laboratory validation for consistent ozone intensities in the MW, 10 and 5 μm ranges.  
407       The Journal of Chemical Physics, 150(18), 184303. <https://doi.org/10.1063/1.5089134>, 2019.
- 408
- 409
- 410



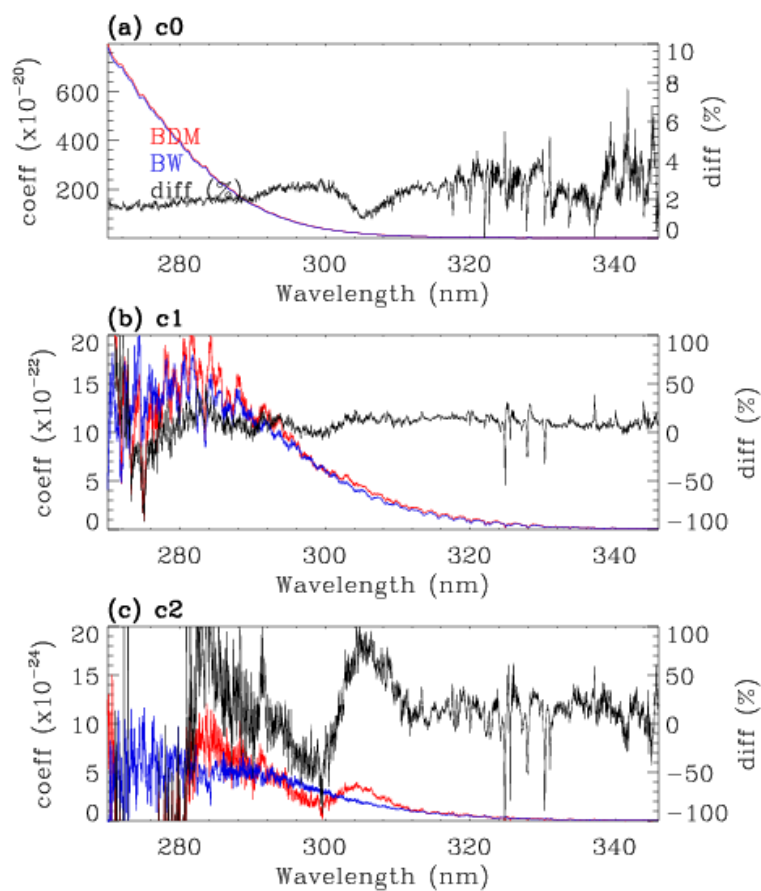
411

412 **Figure 1. (Left) Measurements of ozone absorption cross-sections at all selected temperatures in**  
413 **the Huggins bands taken from (a) BW (2018) and (b) BDM (1995), respectively. (Right) For BW,**  
414 **the experimental data are plotted without the quadratic parameterization for a fair comparison**  
415 **with BDM. BDM measurements at 273 K are plotted with a dotted line on the left and with open**  
416 **circles on the right, because the data at this temperature are not recommended for use, by Liu et**  
417 **al. (2007).**

418

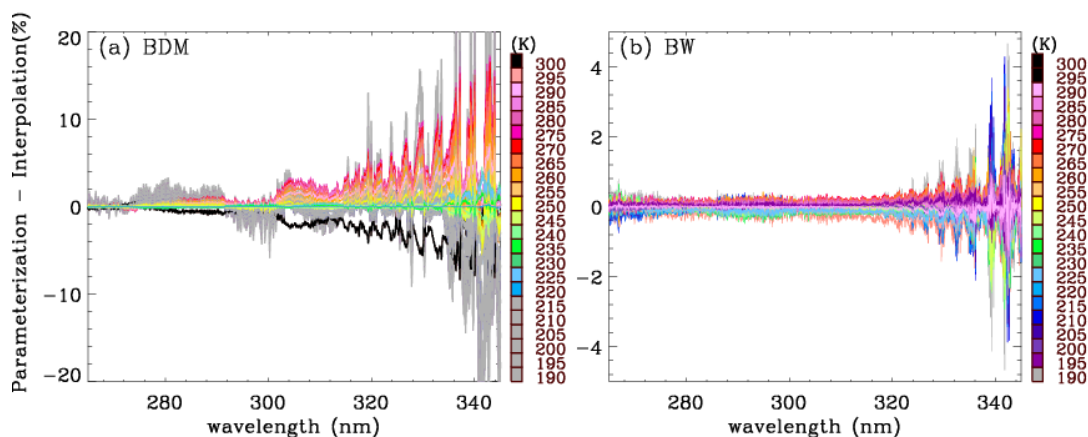
419

420



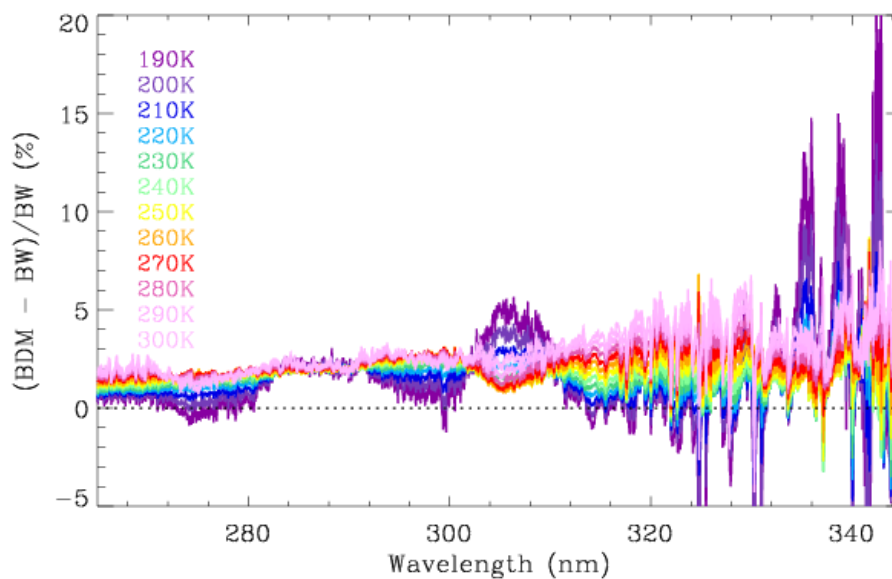
421

422 **Figure 2. Quadratic coefficients ( $\text{cm}^2/\text{molecule}$ ) to parameterize the temperature dependence of**  
423 **ozone cross-sections for BDM (red) and BW (blue), respectively, with their relative differences**  
424 **(BDM-BW)/BW in black.**



425

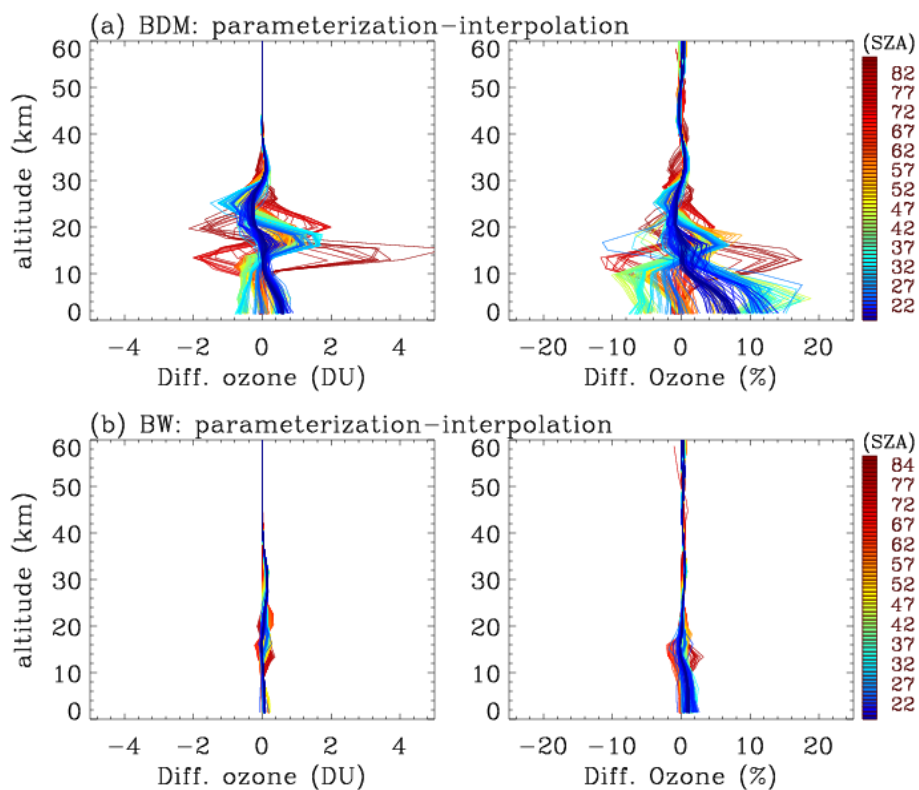
426 **Figure 3.** Relative differences of ozone cross-sections parameterized and spline interpolated at  
427 **temperatures between 190 and 300 K, for (a) BDM and (b) BW, respectively.** In the legend, the  
428 **temperatures not covered by each dataset are indicated with gray and black, for values beyond**  
429 **lower and upper boundaries, respectively.**



430

431 **Figure 4.** Same as Figure 3, but for relative differences (%) of parameterized ozone cross-sections  
432 **between BDM and BW.**

433

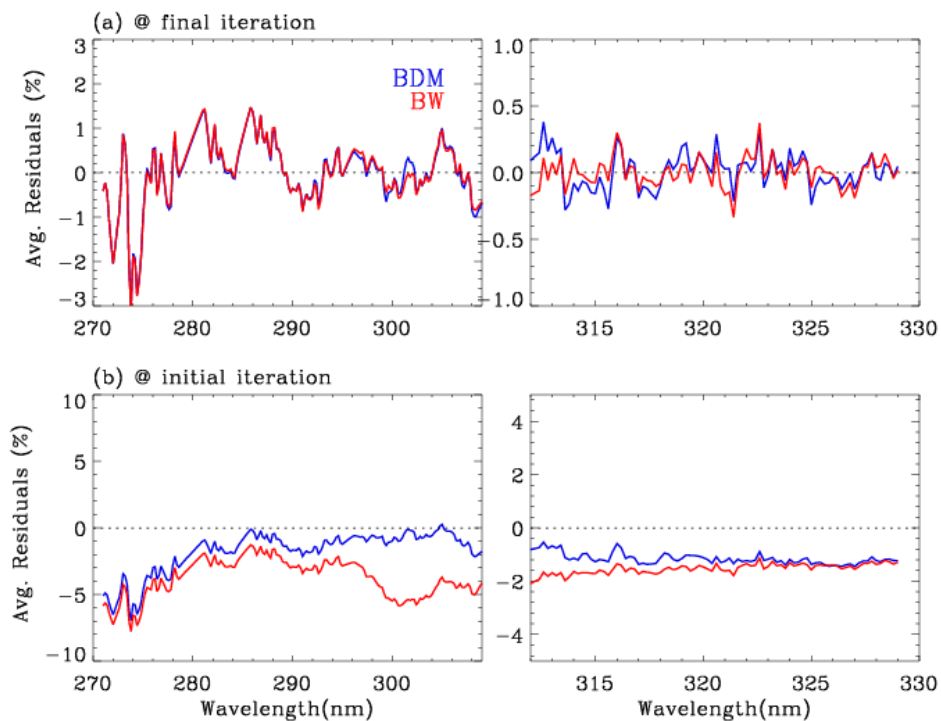


434

435 **Figure 5. The impact of parameterizing the cross-sections shown in Figure 3 on ozone profile**  
436 **retrievals, for (a) BDM and (b) BW.**

437

438

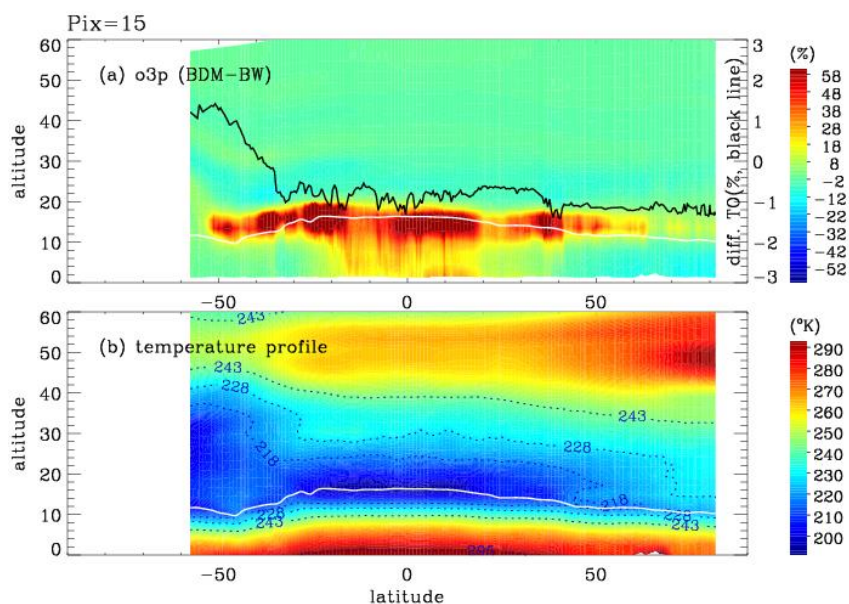


439

440 **Figure 6. Comparison of mean fitting residuals at latitudes of 15° S to 15° N at (a) final iteration**  
441 **and (b) initial iteration, respectively, when using BDM (blue) and BW (red).**

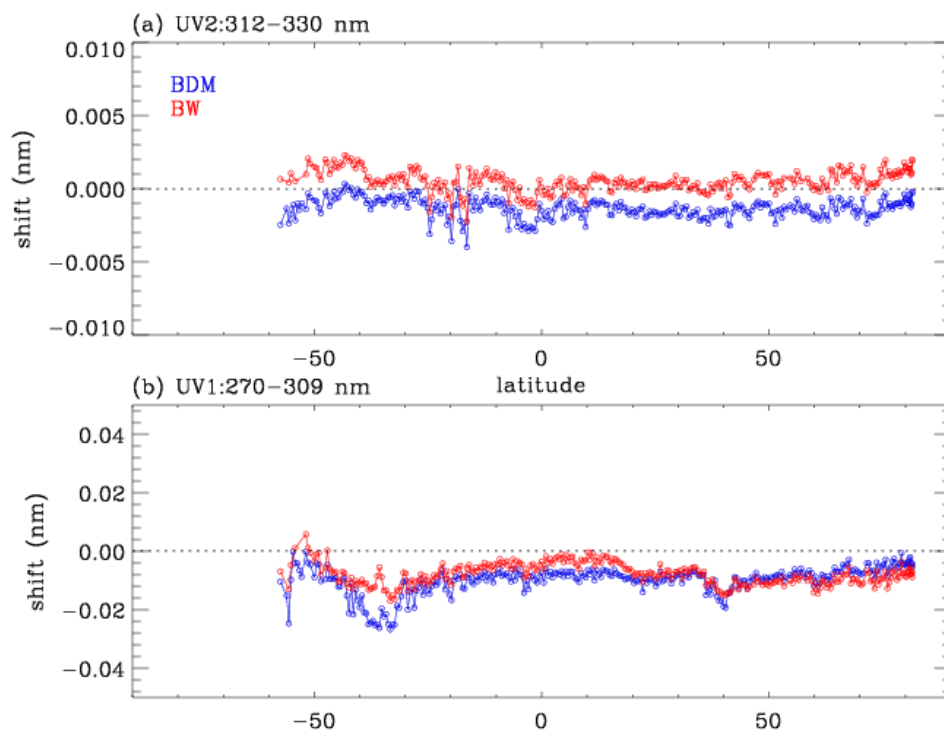
442

443



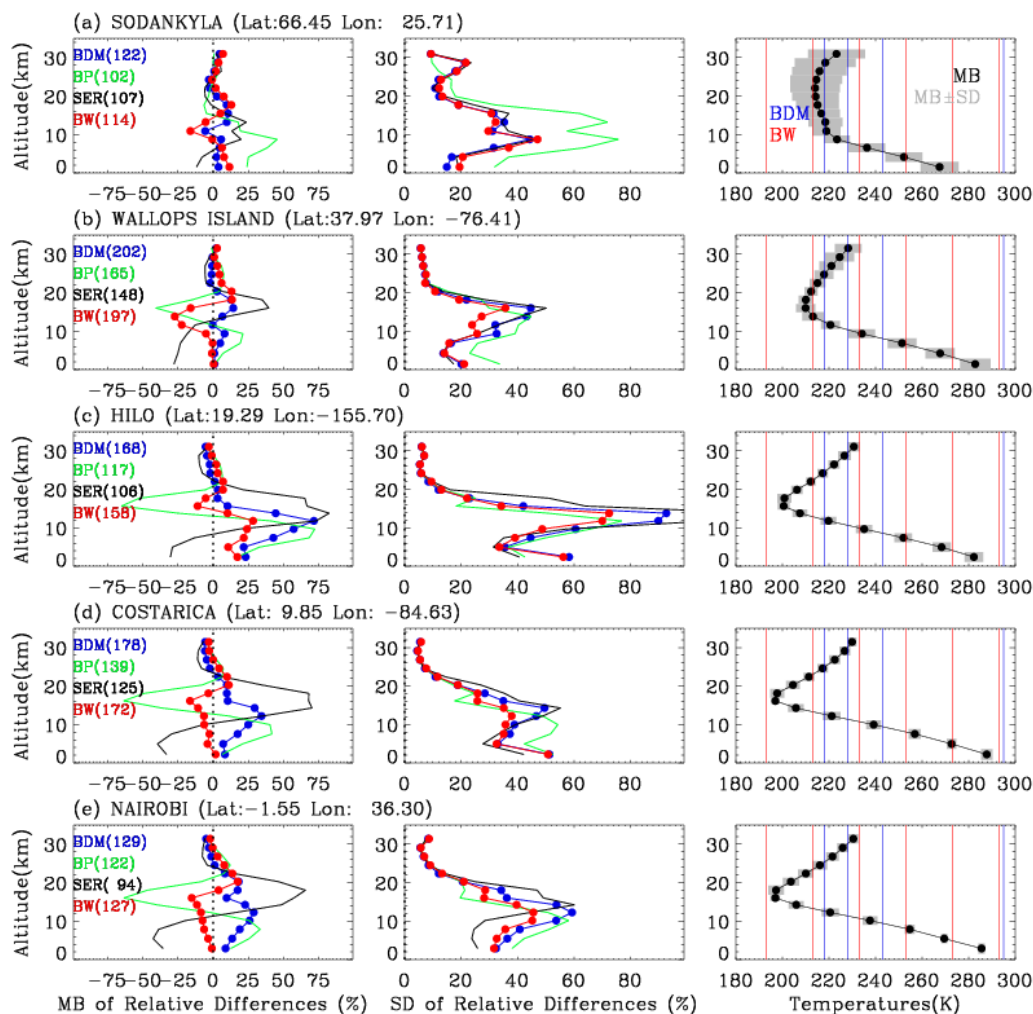
444

445 **Figure 7. (a) Percent Difference  $((BDM-BW)/BW \times 100\%)$  of retrieved ozone profiles using BDM**  
446 **and BW datasets at nadir view, and (b) corresponding temperature profiles in the retrievals. In the**  
447 **upper panel, the black line represents the differences of integrated column ozone. The white line**  
448 **in both panels represents the tropopause height.**



449

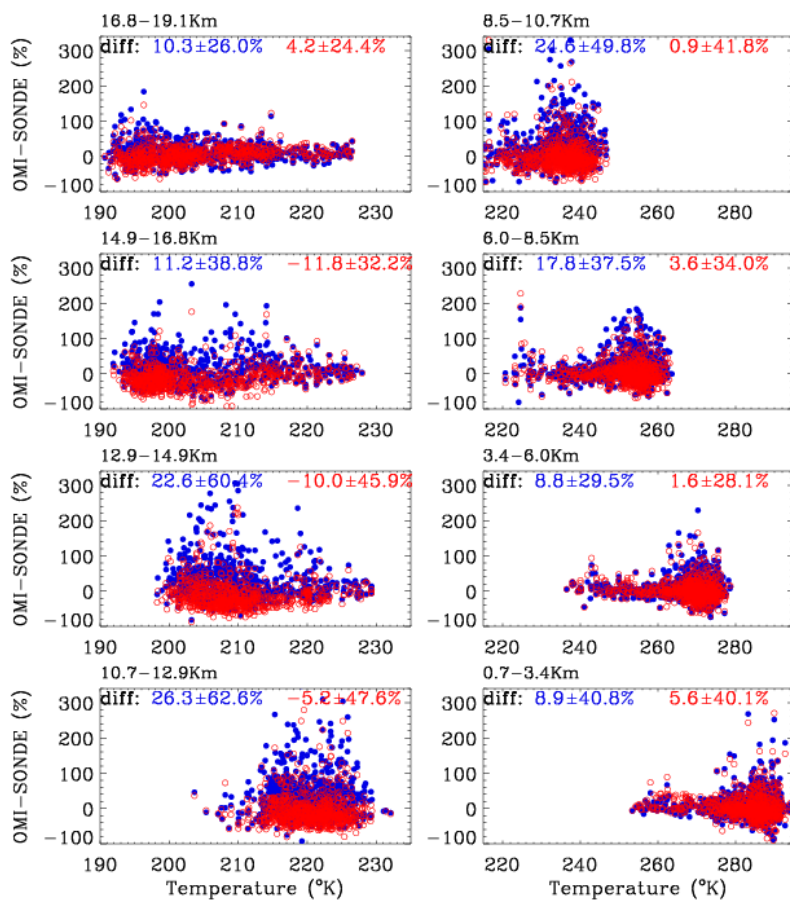
450 **Figure 8.** Comparison of the wavelength shifts (nm) between ozone cross-sections and OMI  
451 radiances at the nadir view for using BDM (blue) and BW cross-sections, respectively.



452

453 **Figure 9. (Left column) Mean biases of relative differences between OMI and ozonesonde ozone**  
 454 **profiles at five stations arranged with decreasing latitude when four different cross-sections are**  
 455 **applied to OMI retrievals, with (Middle column) the corresponding standard deviations and (Right**  
 456 **column) mean temperatures (black circle) of individual profiles (gray). The numbers after the four**  
 457 **cross-sections in the legends show the number of successful retrievals. Blue and red vertical colors**  
 458 **in the right panels represent the temperatures used to derive the quadratic coefficients from BDM**  
 459 **and BW measurements, respectively.**

460



461

462 **Figure 10. Scatter plots of individual differences between OMI retrievals using BDM (blue) and BW**  
463 **(red) cross-sections and ozonesonde measurements for each layer from the surface (bottom right)**  
464 **to 19.1 km (top left) as functions of layer temperature. Mean differences and standard deviations**  
465 **for both cross-sections are shown in the legends.**

466